Voltage-modulated van der Waals interaction in single-molecule junctions

Yujing Wei^a, Liang Li^a, Julia E. Greenwald^a, Latha Venkataraman*a,b

^aDepartment of Chemistry, Columbia University, New York, New York 10027, United States

^bDepartment of Applied Physics and Applied Mathematics, Columbia University, New York,

New York 10027, United States

Email: lv2117@columbia.edu

ABSTRACT: Understanding how molecular geometry affects the electronic properties of single-

molecule junctions experimentally has been challenging. Typically, metal-molecule-metal

junctions are measured using a break-junction method where electrode separation is mechanically

evolving during measurement. Here, to probe the impact of the junction geometry on conductance,

we apply a sinusoidal modulation to the molecular junction electrode position. Simultaneously, we

probe the nonlinearity of the current-voltage characteristics of each junction through a modulation

in the applied bias at a different frequency. In turn, we show that junctions formed with molecules

that have different molecule-electrode interfaces exhibit statistically distinguishable Fourier-

transformed conductances. In particular, we find a marked bias-dependence for the modulation of

junctions where transmission is mediated thorough the van der Waals (vdW) interaction. We

attribute our findings to voltage-modulated vdW interactions at the single-molecule level.

KEYWORDS: single-molecule, fast Fourier transform, van der Waals interaction, conductance

decay, molecular conformation, molecular junctions

1

Single-molecule junctions are a popular platform in studying molecular electronics. To this end, there have been myriad demonstrations of the electron transport properties of single molecules 1-6. Yet, measuring how the junction geometry affects these devices' conductance remains experimentally difficult, especially at room temperature, due to the short lifetime of a particular conformation at room temperature in break-junction measurements and the challenges of controlling the electrode-molecule interface^{3, 7-14}. Critically, it has been shown that the transport properties of a molecular junction depend on molecular conformation, which is shown to be tunable mechanically and electronically¹⁵⁻²³. To statistically sample over the molecular conductance that could occur in a junction at room temperature, one of the most widely-used experimental techniques for investigating single-molecule junctions is the scanning tunneling microscopy break-junction (STM-BJ) method²⁴. In this method, the properties of a single-molecule junction are measured while the electrode separation is increased to facilitate the formation, evolution, and rupture of the junction. Each measurement therefore samples a progression of numerous distinct conformations. This method has been used before with rigid molecules covalently bonded to electrodes. Here, we show that it can be used to explore distance-dependent intermolecular interactions at the single-molecule level. Importantly, we find that the applied bias between electrodes affects the coupling at the electrode-molecule interface, allowing us to probe sub-molecular interactions through the interplay between the electronic and mechanical properties in single-molecule junctions. These results provide a platform to elucidate the properties of distance-dependent electronic interactions, such as the van der Waals (vDW), at a single-molecule scale via modulating the substructure of a molecular junction.

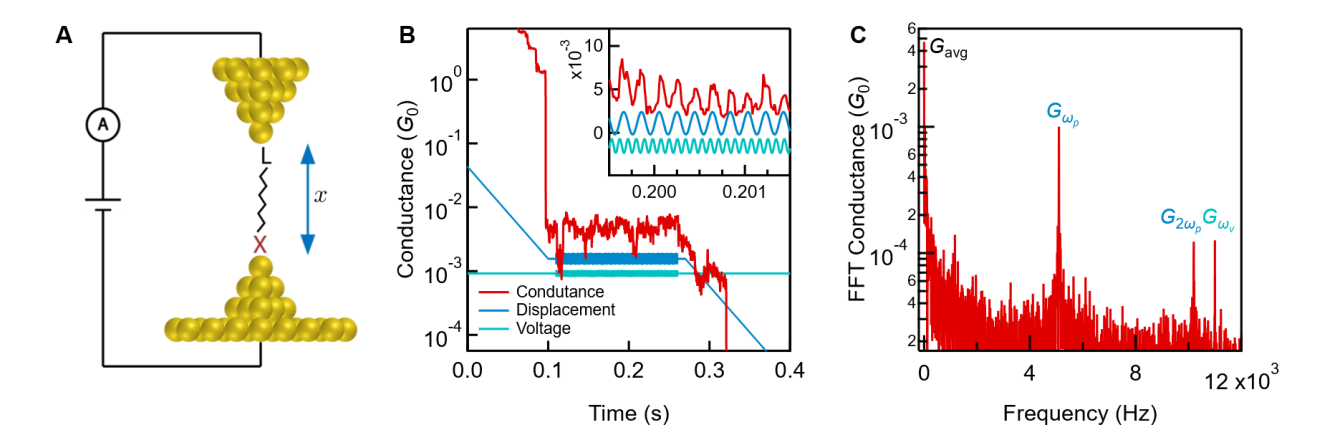


Figure 1. (A) Schematic of the STM-BJ setup for a molecule that binds to gold with linker L and through a van der Waals interaction at X (dark red). The electrode separation is indicated by the distance x. (B) Conductance trace (red) of a single molecular junction. After a fixed time of 0.1 s, the electrode position, or relative displacement (blue) is modulated sinusoidally at a frequency ω_p and 1.2 Å amplitude. The applied voltage (turquoise) is simultaneously modulated at a frequency of ω_v and 26 mV amplitude. Inset: zoomed in view showing conductance response to the modulation. (C) FFT magnitude of the conductance trace. The first and second harmonic peaks of the distance modulation G_{ω_p} and $G_{2\omega_p}$, as well as the first harmonic peak of the bias modulation G_{ω_p} are identified. At zero frequency, the FFT conductance magnitude gives the average conductance of the junction, which we label as G_{avg} .

Herein, we employ a frequency-modulated method with STM-BJ to analyze the effect of distance-dependent molecular interactions on molecular conductance. Figure 1A depicts a molecular junction comprising a general, asymmetric molecule with an aurophilic linker L and a vdW-based interacting site X. The standard STM-BJ technique is described in the Methods section. Figure 1B shows a single trace where the technique has been modified such that after an initial elongation of 2 nm, the junction is held at fixed displacement while the bias and the voltage applied to the piezoelectric transducer are modulated at frequencies ω_v and ω_p , respectively. The molecular junction formation is indicated by a conductance plateau after the rupture of the gold

contact at conductance around $1G_0$, where $G_0 = 2e^2/h$ is the conductance quantum. While the junction is held, the electrode separation x can be described as:

$$x = x_0 + x_1 \sin(\omega_p t + \delta) \tag{1}$$

where x_1 is a small amplitude modulation, x_0 is the mean separation, t is time and δ is the phase. Simultaneously, during this hold, the applied bias can be described as:

$$V = V_0 + V_1 \sin(\omega_v t + \delta) \tag{2}$$

where V_1 is a small voltage modulation, and V_0 is the mean applied bias. This method thus allows the measurement of both mechanically-modulated and electronically-modulated properties of the junction, which we connect in the analysis. The sinusoidal modulations in electrode separation and applied bias prompt sinusoidal responses in the conductance at frequencies ω_p and ω_v respectively, as depicted in the inset of Figure 1B. A fast Fourier Transform (FFT) of the measured conductance during the hold is performed to isolate the effect of modulations on conductance. For $\omega_p = 5.1$ kHz, $x_1 = 1.2$ Å $\omega_v = 11$ kHz, and $V_1 = 26$ mV (see SI section 1 for details), the magnitude of the FFT of conductance displays clear peaks at the modulation frequencies G_{ω_p} and G_{ω_v} as shown in Figure 1C. The second harmonic peak at $2\omega_p$ is also well resolved. Furthermore, the zero-frequency peak is identified as having a conductance of G_{avg} , the average conductance of the junction during the hold. In each experiment, we analyze statistically the Fourier transform of thousands of traces selected using an automated algorithm (see Methods for details).

The magnitude of the FFT of conductance at ω_p is a quantitative indication of the change in conductance with electrode separation. For a tunnel junction, where the two electrodes are

gapped without the presence of a molecule, conductance decays exponentially with the electrode separation as:

$$G = G_C e^{-\beta x} \tag{3}$$

where G is the conductance of the junction, G_C is the exponential prefactor, and β is the conductance decay factor. As a first approximation, to quantify the dependence of single-molecule junction conductance with respect to electrode separation, we replace β with b. The reason behind distinguishing b from β is to distinguish single-molecule junction distance modulation from the decay constants of oligomer series reported in literature — a point that is elaborated on further below. From Taylor expanding Eq. 3 about x_0 , as long as b is independent of x, we obtain:

$$G(t) = G_C e^{-bx_0} \left[\left(1 + \frac{\xi^2}{4} + \frac{\xi^4}{64} + \frac{\xi^6}{2304} + \cdots \right) - \sin(\omega_p t + \delta) \cdot \left(\xi + \frac{\xi^3}{8} + \frac{\xi^5}{192} + \ldots \right) - \cos(2\omega_p t + 2\delta) \cdot \left(\frac{\xi^2}{4} + \frac{\xi^4}{48} + \frac{\xi^6}{1536} + \ldots \right) + \cdots \right] = G_{avg} + G_{\omega_p} + G_{2\omega_p} + \cdots$$

$$(4)$$

where we define a factor $\xi = bx_1$. Eq. 4 shows the result of the Taylor expansion up to the second harmonic term and up to 6^{th} order in ξ . Assuming $\xi < 1$, which is the usual case in tunnel junctions, the ratio of the magnitudes of the first harmonic term to the zeroth harmonic term approaches ξ , i.e., $G_{\omega_p}/G_{avg} \approx \xi$, since G_{avg} is equal to the zeroth order harmonic term in the FFT of conductance. Therefore, the effective conductance decay writes:

$$b = \frac{\xi}{x_1} \approx \frac{1}{x_1} G_{\omega_p} / G_{avg} \tag{5}$$

which is the magnitude of the FFT of conductance at ω_p , normalized by the average conductance and piezo modulation amplitude. This shows that b represents the normalized sensitivity of a molecular junction's conductance to electrode separation which is not the same as β in Eq. 3.

We now apply this analysis to measurements with two different molecules, 4,4'di(methylthio)stilbene (1), and 4-(methylthio)stilbene (2). The chemical structures of 1 and 2 are shown in Figure 2A and their syntheses have been described previously²⁶. Molecule 1 binds to the Au electrodes through Au-SMe donor-acceptor bonds while molecule 2 binds through an Au-SMe bond on one end and a π -Au vdW interaction on the other end. We first measure the conductance of both 1 and 2 without the added junction bias and piezo modulation. Conductance histograms constructed from standard break-junction measurements are shown in Figure 2B and are consistent with published results^{26, 27}. The conductance of 1 is roughly a factor of 50 higher than that of 2, which is largely a reflection of the through-bond nature of the transport in 1 and the through-space coupled transport in 2^{26, 27}. We next measure both molecules while modulating the displacement and bias voltage as described above and analyze the response of conductance to the modulation for traces selected to sustain a molecular junction during the hold segment (see Methods). For each trace, we determine G_{avg} and b (defined in Eq. 5) and construct a 2D histogram with the values from all selected traces of 1 and 2. These histograms are shown in Figures 2C and 2D where we find no correlation between G_{avg} and b nor between x_1 and b (see Figure S4) – the parameter bobtained from the model in Eq. 3 intrinsically normalizes the conductance response by average conductance and modulation amplitude for small modulations. Figure 2E shows a comparison of the parameter b for 1 and 2 on the same axis. The higher response of 2 to distance modulation is indicative of the through-space coupling between the molecular backbone and the electrode, which leads to larger changes in conductance with modulation. The most probable value of b, i.e., the maxima of the distribution in Figure 2E was 0.25 ± 0.03 Å⁻¹ for 1 and 0.63 ± 0.08 Å⁻¹ for 2, where the reported errors are obtained from the histogram bin size. Note that this decay parameter

should not be confused with β in Eq. 3, the decay parameter determined from measuring the conductance of a series of molecules with increasing length, as will be discussed further.

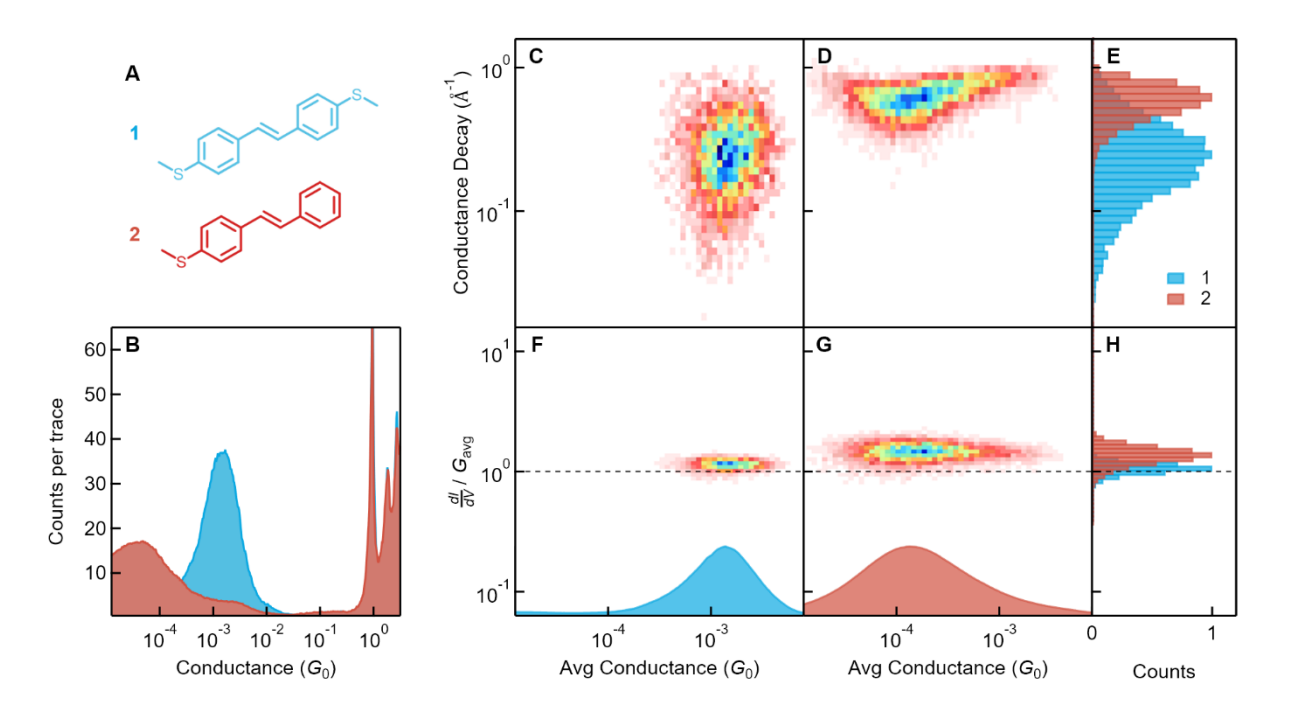


Figure 2. (A) Chemical structures of 1 (blue) and 2 (red). (B) Conductance histograms of constant-pull measurements of 1 (blue) and 2 (red). (C), (D) 2D histograms of the effective exponential conductance decay, b, against the average conductance during the hold portion of each selected trace, G_{avg} , of 1 and 2, respectively. (E) 1D histograms of b for 1 and 2. (F), (G) 2D histograms of the normalized dI/dV against G_{avg} of 1 and 2 respectively. (H) 1D histograms of the normalized dI/dV for 1 and 2. All measurements from (B) to (H) are carried out at 500 mV (average) applied bias.

To further quantify the conductance decay properties, we elaborate on the physical significance of b by ascertaining to what degree the exponential decay model used above is appropriate. To do this, we examine the magnitude of the second harmonic of the FFT magnitude of the conductance, and compare this with that of the first harmonic (see SI section 3). From the Taylor expansion shown in Eq. 4, at small ξ ,

$$G_{2\omega_p}/G_{\omega_p} \approx \frac{1}{4} G_{\omega_p}/G_{avg} \approx \frac{\xi}{4}$$
 (6)

We first test this relation by repeating the modulation measurements with tunnel junctions. We find, as shown in Figure S5A, Eq. 6 holds in excellent agreement with the exponential model. However, for molecular junctions, there is considerable deviation from this model, as seen from Figures S5B and S5C. These results indicate that the exponential conductance decay model (Eq. 3) cannot be used to fully explain the decay in conductance with distance within a single junction, as has been done before $^{10, 11}$. Importantly, we note that b is not constant with respect to junction separation x for a junction with a single molecule. Hence, conductance decay with length for a molecular series and conductance decay with the or electrode separation for a single-molecule junction are not quantitatively following the same decay factor. However, the value of b over thousands of junctions displays no correlation with conductance (Figures 2C, 2D, and S4). Therefore, whilst b using this model is normalized with respect to junction conductance and therefore can be used to compare different junctions, the physical significance of b should not be confused with conventional length-dependent tunneling. Indeed, molecule 1 (Figure S5C) shows higher deviation than molecule 2 (Figure S5B) despite the two molecules having the same backbone. This indicates that through-bond contacts of the molecule with the electrode contribute more to the deviation from the exponential decay model than through-space tunneling or the molecular backbone. Therefore, we suggest that the origin of the conductance change with mechanical modulation is the result of changes in coupling between the molecule and electrode as the metal-molecule interface is mechanically perturbed, altering the geometrical sub-structure of the junction.

We next examine the response of the current to the voltage modulation that is applied simultaneously with the mechanical modulation and determine the differential conductance as:

$$\frac{dI}{dV} = \frac{1}{V_0} I_{\omega_v} \tag{7}$$

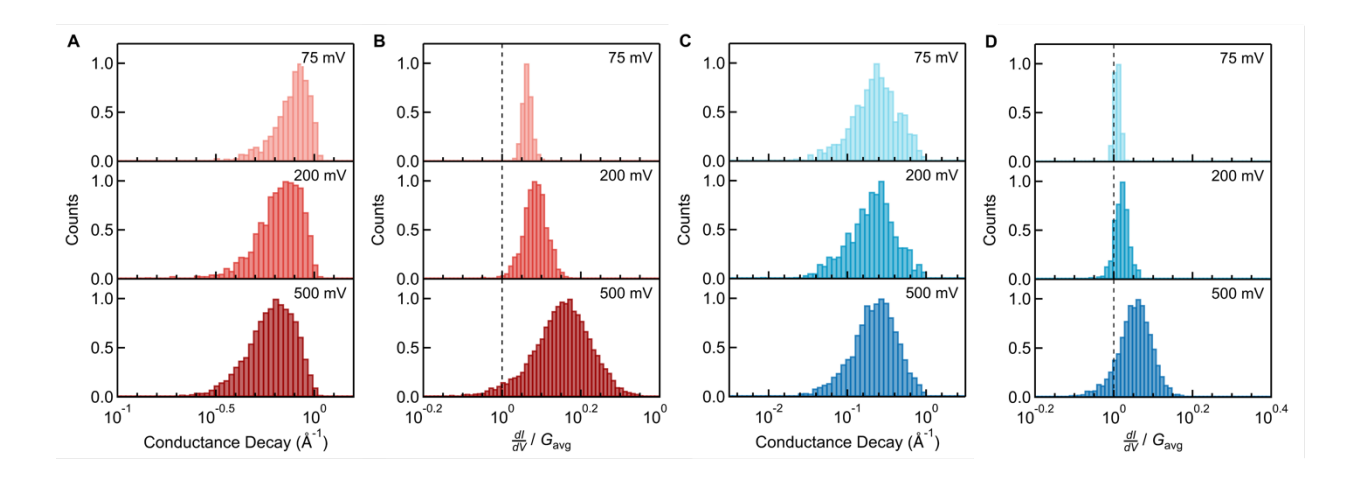


Figure 3. (A) 1D histograms of the effective exponential conductance decay, and (B) 1D histograms of the dI/dV normalized by average junction conductance of 2 at different average applied biases V_0 as labelled in each panel, all with the same modulation voltage amplitude of $V_1 = 26 \text{ mV}$. (C) 1D histograms of the effective exponential conductance decay, and (D) 1D histograms of the dI/dV normalized by average junction conductance of 1 at different average applied biases V_0 , with $V_1 = 26 \text{ mV}$. All histogram counts are normalized to 1.

where I_{ω_v} is the FFT magnitude of the measured current at ω_v . Due to capacitive²⁸ effects in the junction, we take only the in-phase component of the current. Figures 2F and 2G show 2D histograms of the differential conductance normalized by the average conductance, against the average conductance. The normalized differential conductance is larger than 1.0 for both molecules indicating a non-linear I-V characteristic at a DC bias voltage. Additionally, the normalized differential conductance is larger for 2 compared to 1 as can be seen in Figure 2H which shows the same data in a 1D histogram. Since the conductance of 2 has a higher response to both piezo modulation and bias modulation, we propose that through-space molecule-electrode coupling is more susceptible than through-bond coupling to voltage modulations. This is further supported by data using another molecular system as provided in SI section 4, confirming that our method can distinguish between through-space and through-bond coupled molecular junctions.

We now investigate the effect of an applied bias on the vdW mediated through-space coupling. We repeat the modulation measurements while changing the DC bias applied during the mechanical modulation. We then determine the conductance decay parameter *b* at different biases for **2**. As shown in Figure 3A, *b* decreases with increasing applied bias, which implies that the junction is less susceptible to mechanical modulation with increasing voltage. By contrast, the normalized differential conductance increases with increasing bias (Figure 3B) indicating higher nonlinearity of I-V relationship. Remarkably, the effective decay constant and the differential conductance changes markedly with bias for **2** (Figures 3C and 3D respectively) as opposed to **1** which is bound to the junction through donor-acceptor bonds²⁶. Hence, the voltage is able to tune the through-space van der Waals coupling between the molecule and the electrode. This is an exciting demonstration of the modulation of van der Waals interactions at a single-molecule scale.

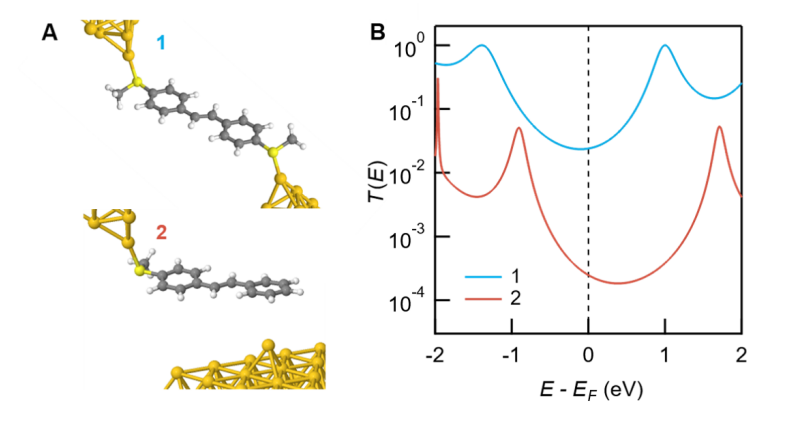


Figure 4. (A) Optimized geometry of 1 (top) and 2 (bottom) in the junction. Note that there is no clear bond between 2 and the bottom electrode. (B) Transmission functions of 1 (blue) and 2 (red).

To explain this phenomenon, we turn to Density Functional Theory (DFT) calculations of the transport properties of single molecules using the FHI-aims software²⁹ (see Methods for details). Figure 4A depicts the optimized geometries of junctions comprising 1 and 2. Using these

optimized geometries, we calculate transmission functions using a non-equilibrium Green's function (NEGF) formalism implemented in the AITRANSS package^{30, 31}. The transmission calculations are shown in Figure 4B. The trends in the transmission values at Fermi agree well with the experiment, i.e. the conductance of 1 is greater than 2, but we note that transport DFT calculations overestimate actual conductance values for many-electron molecules^{32, 33}. The asymmetric coupling of the molecule to the left and right electrodes for 2 results in a peak transmission of less than 10° . The resonance peak for 2 closest to the Fermi energy (E_F) is closer than that for 1 and the slope of the transmission function at E_F is also greater for 2. This explains the larger normalized differential conductance measured for 2 when compared with 1, as the transmission for 2 is more non-linear around E_F . The increasing non-linearity with bias for 2 (Figure 3B) is also due to this feature in the transmission function; the applied bias modifies the coupling, which modifies the width of the resonance^{34, 35}, which modifies the slope and curvature of the transmission at E_F . Specifically, we propose that a larger applied bias facilitates stronger vdW coupling between the benzene and the gold electrode, which results in higher curvature of the transmission at E_F . The stronger coupling is also consistent with the effective decay factor, b, decreasing with increasing bias (Figure 3A). This strengthening of the coupling cannot solely be explained by polarization of the molecule under the electric field (see SI section 5), which further suggests that the bias modulates the vdW interaction.

In conclusion, we have demonstrated a method to statistically probe the response of a single-molecule junction to a change in electrode separation and voltage. We show that using this method, single-molecule junction properties can be distinguished by the magnitude of their Fourier Transforms. Furthermore, we are able to calculate a decay constant for the distance-dependent conductance of a single molecule, whilst simultaneously obtaining the differential conductance of

each trace. We connect these observations with the sub-molecular changes in geometry responsible for the conductance change, which distinguish through-space and through-bond interactions. Critically, the van der Waals junctions show a voltage-modulated behavior, while the donor-acceptor bonded junctions do not. This method and these findings provide new insights into the relationship between junction structure and transport properties.

METHODS:

STM-BJ. The scanning tunneling microscopy break-junction (STM-BJ) technique involves the automated process of repeated formation and rupture of Au-Au contacts between a gold tip (0.25 mm diameter, >99.9% Alfa Aesar) and gold-coated steel substrate (~100 nm thick, >99.9% Alfa Aesar), which form the two electrodes. The gold substrates are UV/ozone cleaned for 20 min before use. Prior to measuring analyte, the substrate is tested for cleanness by measuring 1,000 traces of clean Au without any added solution. During the measurement, a constant bias, V, is applied across the junction with a 100 k Ω resistor in series. The current, I, is measured at an acquisition rate of 100 kHz. Conductance (G=I/V) is measured as a function of displacement in units of G_0 (a conductance quantum, $G_0 = 2e^2/h$). The formation of a bulk Au-Au contact (contact threshold $5G_0$) marks the start of a trace, after which during a constant-pull measurement (see main text for "hold" measurement), the tip is withdrawn from the substrate at a constant speed of 16 nm/s using a piezoelectric actuator until the measured current drops to instrument noise. All measurements are performed under room temperature and atmospheric pressure, with molecules in a solution environment (100 μM in 1,2,4-trichlorobenzene). The measured traces are then collected and compiled into 1D and 2D histograms.

Data analysis. The hold measurements use an automated trace selection and Fourier analysis process. For each measurement, we take tens of thousands of traces. Traces are excluded based on

the following criteria: a) if the conductance during the hold is not bounded by the Gaussian distribution of the molecule's conductance from the 1D conductance histogram, b) if the conductance during the hold varies by more than 1.5 orders of magnitude indicating abrupt conformation change in the junction c) if the conductance at the beginning of the hold is more than half an order of magnitude different from the conductance at the end of the hold to ensure closeness to periodicity of the hold region. For each selected trace, the same region of the hold is Fourier transformed using the FFT function in IgorPro.

DFT calculations. The Perdew-Burke-Ernzerhof (PBE) exchange-correlation functional³⁶ was used for the DFT steps, with atomic zeroth-order regular approximation (ZORA)³⁷ for scalar relativistic corrections to the kinetic energy, using a "double Zeta plus polarization"-equivalent basis set for non-gold atoms, and "double Zeta"-equivalent basis set for gold atoms. The transmission function is calculated using a non-equilibrium Green's function (NEGF) formalism implemented in the AITRANSS package^{30, 31}. The calculation procedure proceeded in a geometry optimization, followed by a transmission calculation. As a first step, the geometry of the molecule attached to one gold atom on each side was optimized. We then take this optimized structure and append two gold pyramidal clusters with three additional layers (three, six, and ten atoms respectively) on top of the single gold atoms, along with two additional adatoms with randomized positions to introduce a little asymmetry into the gold clusters. Calculation of molecule 2 involved constraining the gold adatom on the linker-less side of the molecule to a triangular slab (two layers of 15 and 21 gold atoms) during the first step of geometry optimization, since a single gold atom has an unpaired electron, and without a molecular linker, the gold will over-bind to carbon. The single gold adatom that interacts with the benzene ring on the linker-less side is then added to the slab; upon another optimization we see negligible geometry change, indicating the π -Au

interaction is through-space and delocalized. For the side with the thiomethyl linker, the optimization procedure is the same as for molecule 1.

Associated content

Supporting information

STM-BJ measurement details and additional experimental and theoretical data. This material is available free of charge at https://pubs.acs.org.

Author Information

Corresponding Authors

Latha Venkataraman – Department of Chemistry and Department of Applied Physics and Applied Mathematics, Columbia University, New York, New York 10027, United States; orcid.org/0000-0002-6957-6089; Email: lv2117@columbia.edu

Authors

Yujing Wei – Department of Chemistry, Columbia University, New York, New York 10027, United States; orcid.org/0000-0001-8913-9719; Email: yw3557@columbia.edu

Liang Li – Department of Chemistry, Columbia University, New York, New York 10027, United States; orcid.org/0000-0003-3890-7276; Email: ll3332@columbia.edu

Julia E. Greenwald – Department of Chemistry, Columbia University, New York, New York 10027, United States; Email: jeg2219@columbia.edu

Notes

The authors declare no competing financial interests.

Acknowledgements

This work was supported in part by the NSF CHE-2023568 CCI Phase I: Center for Chemistry with Electric Fields and by NSF DMR-1807580.

References.

- (1) Reed, M. A.; Zhou, C.; Muller, C. J.; Burgin, T. P.; Tour, J. M., Conductance of a molecular junction, *Science*, **1997**, 278, 252-254.
- (2) Aradhya, S. V.; Venkataraman, L., Single-molecule junctions beyond electronic transport, *Nat. Nanotechnol.*, **2013**, 8, 399-410.
- (3) Gehring, P.; Thijssen, J. M.; van der Zant, H. S. J., Single-molecule quantum-transport phenomena in break junctions, *Nat. Rev. Phys.*, **2019**, 1, 381-396.
- (4) Huang, C.; Rudnev, A. V.; Hong, W.; Wandlowski, T., Break junction under electrochemical gating: testbed for single-molecule electronics, *Chem. Soc. Rev.*, **2015**, 44, 889-901.
- (5) Komoto, Y.; Fujii, S.; Iwane, M.; Kiguchi, M., Single-molecule junctions for molecular electronics, *Journal of Materials Chemistry C*, **2016**, 4, 8842-8858.
- (6) Evers, F.; Korytár, R.; Tewari, S.; van Ruitenbeek, J. M., Advances and challenges in single-molecule electron transport, *Rev. Mod. Phys.*, **2020**, 92, 035001.
- (7) Haiss, W.; Wang, C. S.; Grace, I.; Batsanov, A. S.; Schiffrin, D. J.; Higgins, S. J.; Bryce, M. R.; Lambert, C. J.; Nichols, R. J., Precision control of single-molecule electrical junctions, *Nat. Mat.*, **2006**, 5, 995-1002.
- (8) Quek, S. Y.; Kamenetska, M.; Steigerwald, M. L.; Choi, H. J.; Louie, S. G.; Hybertsen, M. S.; Neaton, J. B.; Venkataraman, L., Mechanically Controlled Binary Conductance Switching of a Single-Molecule Junction, *Nat. Nanotechnol.*, **2009**, 4, 230-234.

- (9) Wu, S. M.; Gonzalez, M. T.; Huber, R.; Grunder, S.; Mayor, M.; Schonenberger, C.; Calame, M., Molecular junctions based on aromatic coupling, *Nat. Nanotechnol.*, **2008**, 3, 569-574.
- (10) Bruot, C.; Hihath, J.; Tao, N., Mechanically controlled molecular orbital alignment in single molecule junctions, *Nat. Nanotechnol.*, **2011**, 1-6.
- (11) Rascón-Ramos, H.; Artés, J. M.; Li, Y.; Hihath, J., Binding configurations and intramolecular strain in single-molecule devices, *Nat. Mat.*, **2015**.
- (12) Komoto, Y.; Fujii, S.; Nakamura, H.; Tada, T.; Nishino, T.; Kiguchi, M., Resolving metal-molecule interfaces at single-molecule junctions, *Sci. Reps.*, **2016**, 6, 1-9.
- (13) Stefani, D.; Weiland, K. J.; Skripnik, M.; Hsu, C.; Perrin, M. L.; Mayor, M.; Pauly, F.; van der Zant, H. S. J., Large Conductance Variations in a Mechanosensitive Single-Molecule Junction, *Nano Lett.*, **2018**, 18, 5981-5988.
- (14) Camarasa-Gomez, M.; Hernangomez-Perez, D.; Inkpen, M. S.; Lovat, G.; Fung, E. D.; Roy, X.; Venkataraman, L.; Evers, F., Mechanically Tunable Quantum Interference in Ferrocene-Based Single-Molecule Junctions, *Nano Lett.*, **2020**, 20, 6381-6386.
- (15) Moresco, F.; Meyer, G.; Rieder, K. H.; Tang, H.; Gourdon, A.; Joachim, C., Conformational changes of single molecules induced by scanning tunneling microscopy manipulation: A route to molecular switching, *Phys. Rev. Lett.*, **2001**, 86, 672-675.
- (16) Dulic, D.; van der Molen, S. J.; Kudernac, T.; Jonkman, H. T.; de Jong, J. J. D.; Bowden, T. N.; van Esch, J.; Feringa, B. L.; van Wees, B. J., One-way optoelectronic switching of photochromic molecules on gold, *Phys. Rev. Lett.*, **2003**, 91, 207402.
- (17) Salomon, A.; Cahen, D.; Lindsay, S.; Tomfohr, J.; Engelkes, V. B.; Frisbie, C. D., Comparison of electronic transport measurements on organic molecules, *Adv. Mater.*, **2003**, 15, 1881-1890.

- (18) Venkataraman, L.; Klare, J. E.; Nuckolls, C.; Hybertsen, M. S.; Steigerwald, M. L., Dependence of single-molecule junction conductance on molecular conformation, *Nature*, **2006**, 442, 904-907.
- (19) Mishchenko, A.; Zotti, L. A.; Vonlanthen, D.; Burkle, M.; Pauly, F.; Cuevas, J. C.; Mayor, M.; Wandlowski, T., Single-Molecule Junctions Based on Nitrile-Terminated Biphenyls: A Promising New Anchoring Group, *J. Am. Chem. Soc.*, **2011**, 133, 184-187.
- (20) French, W. R.; Iacovella, C. R.; Rungger, I.; Souza, A. M.; Sanvito, S.; Cummings, P. T., Atomistic simulations of highly conductive molecular transport junctions under realistic conditions, *Nanoscale*, **2013**, 5, 3654-3659.
- (21) Kim, Y.; Garcia-Lekue, A.; Sysoiev, D.; Frederiksen, T.; Groth, U.; Scheer, E., Charge Transport in Azobenzene-Based Single-Molecule Junctions, *Phys. Rev. Lett.*, **2012**, 109, 226801-226801.
- (22) Wu, C., et al., Folding a Single-Molecule Junction, *Nano Lett.*, **2020**, 20, 7980-7986.
- (23) Tang, C., et al., Electric-Field-Induced Connectivity Switching in Single-Molecule Junctions, *iScience*, **2020**, 23, 100770.
- (24) Xu, B. Q.; Tao, N. J., Measurement of single-molecule resistance by repeated formation of molecular junctions, *Science*, **2003**, 301, 1221-1223.
- (25) Bruot, C.; Palma, J. L.; Xiang, L.; Mujica, V.; Ratner, M. A.; Tao, N., Piezoresistivity in single DNA molecules, *Nat. Commun.*, **2015**, 6, 8032.
- (26) Meisner, J. S.; Ahn, S.; Aradhya, S. V.; Krikorian, M.; Parameswaran, R.; Steigerwald, M.; Venkataraman, L.; Nuckolls, C., Importance of Direct Metal–π Coupling in Electronic Transport Through Conjugated Single-Molecule Junctions, *J. Am. Chem. Soc.*, **2012**, 134, 20440-20445.

- (27) Adak, O.; Rosenthal, E.; Meisner, J.; Andrade, E. F.; Pasupathy, A. N.; Nuckolls, C.; Hybertsen, M. S.; Venkataraman, L., Flicker Noise as a Probe of Electronic Interaction at Metal-Single Molecule Interfaces, *Nano Lett.*, **2015**, 15, 4143-4149.
- (28) Adak, O.; Korytar, R.; Joe, A. Y.; Evers, F.; Venkataraman, L., Impact of Electrode Density of States on Transport through Pyridine-Linked Single Molecule Junctions, *Nano Lett.*, **2015**, 15, 3716-3722.
- (29) Blum, V.; Gehrke, R.; Hanke, F.; Havu, P.; Havu, V.; Ren, X.; Reuter, K.; Scheffler, M., Ab initio molecular simulations with numeric atom-centered orbitals, *Comp. Phys. Commun.*, **2009**, 180, 2175-2196.
- (30) Arnold, A.; Weigend, F.; Evers, F., Quantum chemistry calculations for molecules coupled to reservoirs: Formalism, implementation, and application to benzenedithiol, *J. Chem. Phys.*, **2007**, 126, 174101.
- (31) Bagrets, A., Spin-Polarized Electron Transport Across Metal—Organic Molecules: A Density Functional Theory Approach, *J. Chem. Theory Comput.*, **2013**, 9, 2801-2815.
- (32) Evers, F.; Weigend, F.; Koentopp, M., Conductance of molecular wires and transport calculations based on density-functional theory, *Phys. Rev. B*, **2004**, 69, 235411.
- (33) Neaton, J. B.; Hybertsen, M. S.; Louie, S. G., Renormalization of molecular electronic levels at metal-molecule interfaces, *Phys. Rev. Lett.*, **2006**, 97, 216405.
- (34) Breit, G.; Wigner, E., Capture of Slow Neutrons, *Phys. Rev.*, **1936**, 49, 519.
- (35) Cuevas, J. C.; Scheer, E., *Molecular Electronics: An Introduction to Theory and Experiment*. World Scientific: 2017; Vol. Volume 15, p 848.
- (36) Perdew, J. P.; Burke, K.; Ernzerhof, M., Generalized Gradient Approximation Made Simple, *Phys. Rev. Lett.*, **1996**, 77, 3865-3868.

(37) Van Lenthe, E.; Baerends, E. J.; Snijders, J. G., Relativistic Total-Energy Using Regular Approximations, *J. Chem. Phys.*, **1994**, 101, 9783-9792.